Experimental insights into the stiffness degradation of subgrade soils prone to mud pumping

Authors:

Mandeep Singh[1], Ph.D., Senior Technical Support Officer (GeoTech)

Buddhima Indraratna[2*], Distinguished Professor

Thanh Trung Nguyen[3], Research Fellow

[1]University of Technology Sydney, Tech Lab, Botany NSW 2019, Australia.

[2]School of Civil and Environmental Engineering and Director, Transport Research Centre (TRC), University of Technology Sydney, NSW 2007, Australia

Formerly: Founding Director, Centre for Geomechanics and Railway Engineering; Director, Australian Research Council (ARC) Industrial Transformation Training Centre, ITTC-Rail University of Wollongong, NSW 2522, Australia.

[3]Transport Research Centre (TRC), University of Technology Sydney, NSW 2007, Australia.

Word count: 2637 (excluding references, tables and figures)

Figures: 6

Submitted to: Transportation Geotechnics

[*]Corresponding author: Buddhima Indraratna (e-mail: Buddhima.Indraratna@uts.edu.au)

Abstract

Recent laboratory investigations conducted on soils prone to mud pumping have shown that the subgrade soil experiences softening associated with an internal redistribution of moisture when the cyclic stress ratio (CSR) exceeds a certain critical level. This article aims to evaluate the stiffness degradation of these problematic subgrade soils subjected to a wide range of loading conditions. The test results revealed that the instability of the specimens is caused by the early softening behaviour, and this is accompanied by a sharp reduction in the specimen stiffness. As high as 70-80% reduction in the initial small-strain stiffness was observed even for densely compacted specimens (ρ_d = 1790 kg/m^3). In this regard, a new method for predicting the threshold number of cycles, N_{thr} and residual axial strains required for the onset of subgrade instability is proposed. As a useful practical guide, a quasi-linear relationship between the threshold strain and N_{thr} is also determined.

Keywords: Mud pumping; fluidization; subgrade instability; stiffness degradation.

1. Introduction

In recent times there has been a considerable interest within the railway geotechnical community to investigate the underlying mechanisms and to propose appropriate remediation measures for ballasted tracks affected by mud pumping (Kuo et al., 2017; Hasnayn et al., 2017; Nguyen et al., 2019; Singh et al., 2019; Indraratna et al. 2020a and 2020b). In short, mud pumping is the upward migration of soft subgrade fines to the coarser ballast layer. Indraratna et al. (2020b) reported that low plastic soils can experience fluidization where soil turns into a fluid-like state under the ballast at high applied cyclic stresses and termed it as subgrade fluidization. Few researchers (Nguyen and Indraratna, 2020) have explained the micro-mechanism behind the fluidisation of subgrade soils using advanced CFD-DEM coupling. Indraratna et al. 2020a observed early softening of fluidized specimens at high applied cyclic stresses. Hasnayn et al. 2020 performed full-scale experimental investigations on submerged rail track system and reported that flooding caused a continual reduction in soil stiffness. As the fluidized specimens were unable to sustain the amount of applied cyclic stress and therefore, it is essential to quantify the stiffness of the subgrade specimens under cyclic loading to provide further insight to the degradation aspect of these unstable specimens.

Clay soils in general, when subjected to cyclic loading experience a reduction in the stiffness with the number of loading cycles. On the other hand, coarse-grained soils when subjected to lower cyclic stresses experience an increase in the stiffness due to densification (Leng et al., 2017). Zhou and Gong (2001) proposed a relationship for the strain degradation in terms of the applied cyclic load, the frequency and the over-consolidation ratio. Kallioglou et al. (2008) reported a comprehensive summary of the factors effecting the small-strain shear modulus and studied the role of plasticity index in governing the degradation of the shear modulus.

Although there is an abundance of literature on the degradation of soft soils, majority of them have been carried out for strain-controlled cyclic triaxial tests (Zhou and Gong, 2001; Mortezaie and Vucetic, 2013). Also, it is widely accepted that when fully saturated soils are subjected to large cyclic strain amplitudes under undrained conditions, they experience a permanent change in the soil structure leading to a decrease in the stiffness as well as the strength and a permanent increase in the pore water pressure. The stress path adopted while loading the specimens also plays a crucial role in the stiffness degradation of the specimens. When the specimens are subjected to principal stress rotation, the specimens experience larger strains and thereby severe stiffness degradation (Cai et al. 2018, Mamou et al. 2019). As will be shown later, there exists a correlation between the generation of excess pore pressure and stiffness degradation for fluidized soil specimens, and there are limited studies addressing this phenomenon (Hsu and Vucetic, 2006; Soralump and Prasomsri, 2016). This paper aims to establish the threshold residual axial strains for fluidized specimens by considering in tandem the stiffness degradation index and the mean excess pore pressure ratio$\left(u_{\mathrm{m}}/\sigma'_{3\mathrm{c}}\right)$.

2. Experimental investigation

2.1. Undrained cyclic triaxial testing

The response of two subgrade soils prone to mud pumping was studied by conducting a series of undrained cyclic triaxial tests on remoulded soil specimens, at various initial dry densities (detailed experimental procedures are described elsewhere by Indraratna et al., 2020a; 2020b). The particle size distribution (PSD) of the two soils indicates that these two samples have a high percentage of fines (< 75 μm) of about 30% and 54% for soils - MP1 and MP2, respectively (Fig. 1). The basic geotechnical properties of the soils MP1 and MP2 are detailed in Table 1. The ratio of the initial dry density (ρ_{d}) to that of the maximum dry density as obtained by Standard Proctor test (ASTM D698-07 Standard, 2012) is defined as relative compaction (RC). The cyclic stress ratio (CSR) is defined as the ratio of the amplitude of the applied cyclic stress ($\sigma_d/2$) to that of the effective confining pressure after consolidation (σ'_{3c}).

$$\text{CSR}=\frac{\sigma_d}{2\sigma'_{3c}} \quad (1)$$

The pore pressure transducer installed at the base of the standard triaxial cell was calibrated prior to each test. The specimens were fully saturated to achieve a Skempton's B-value exceeding 0.95 prior to the anisotropic consolidation phase (ratio of effective horizontal stress to the vertical stress, $k_0 = 0.6$). A low effective confining pressure ($\sigma'_{3c} = 15$ kPa) was chosen to represent the shallow regions of the rail subgrade thereby, the initial deviatoric stress, q_0, for the tested specimens was set to 10 kPa. For the tested frequency range (1.0 – 5.0 Hz), the time lag in the peak and trough of the excess pore pressure response corresponding to the applied cyclic load was insignificant. The anticipated stresses on the top of the subgrade were considered to be within the range of 15 to 30 kPa for various axle loads (14-23 t) (Liu and Xiao, 2010). Therefore, the testing was carried out for a wide range of CSR (0.2 to 1.0). It is noteworthy that Powrie et al. (2007) have noted a frequency of 4.0 Hz acting at 1.0 m below the sleeper base for train speed at 50 m/s (180 km/h), implying that the authors' tested frequency range of 1.0 to 5.0 Hz would correspond to train speeds of 45- 225 km/h on standard gauge tracks. The influence of the CSR and loading frequency on the stiffness degradation is highlighted in the following sections and the details of soil properties and loading parameters used in the current study are summarized in Table 2.

2.2. Cyclic response of the soil specimens

Two distinct stress-strain responses, viz., stable and unstable response were recorded as the cyclic stress ratio is increased. As can be seen from Fig. 2a, when the specimen ($\rho_d = 1790$

kg/m^3) was subjected to a CSR = 0.4 at a loading frequency of f = 1.0 Hz, the stress-strain loops stabilized after about 1000 cycles. The maximum cyclic axial strain (ε_{ac}) after 50000 cycles is shown to be only 0.45%. Further, when the CSR is increased to 1.0, the test specimen shows signs of early softening due to which the specimens were unable to withstand the applied cyclic stress (Fig. 2b). These observations clarify that the reduction in the stiffness as observed from the stress-strain loops is more prominent at higher CSR due to the formation of slurry at the top of the fluidized specimen. At CSR greater than the critical cyclic stress ratio (CSR_c), the specimen experiences a rapid increase in the mean excess pore pressure ratio along with a sudden decrease in the stiffness.

3. Stiffness Degradation Index

When soils experience larger strains, there is a significant reduction in the soil stiffness. While some past studies (Zhou and Gong, 2001; Lei et al., 2016) have computed the stiffness degradation by assuming constant level of stress, this may not be applicable for the fluidized specimens as they experience early softening (as indicated in Fig. 2). Therefore, the approach suggested by Cai et al. (2018) was adopted for the current analysis by evaluating the axial dynamic modulus of each loading-unloading cycle.

The generalised behaviour of a soil subjected to one-way stress controlled cyclic loading is depicted in Fig. 3. The axial dynamic stiffness is defined as the ratio of the difference of maximum and minimum deviatoric stress to the difference of the maximum and minimum axial strain at N number of cycles (note that the data logger records 10 data points per cycle):

$$E_{d,N} = \left[\frac{\sigma_{d,max} - \sigma_{d,min}}{\varepsilon_{d,max} - \varepsilon_{d,min}}\right]_N \tag{2}$$

As the axial strains are readily measured in the triaxial setup and have been used to determine the specimen stiffness, the corresponding modulus is termed as the axial dynamic stiffness. The stiffness degradation index, δ, is computed by comparing the axial dynamic stiffness of a given cycle to that of the first cycle, thus:

$$\delta = \frac{E_{d,N}}{E_{d,1}} \tag{3}$$

4. Relationship between the stiffness degradation index and mean excess pore pressure ratio

4.1. Predicting threshold number of cycles, N_{thr}

Konstadinou and Georgiannou (2014) estimated the critical number of cycles for the liquefaction of sands based on the variation in the excess pore water pressure data. The critical number of cycles was estimated by plotting the incremental normalized excess pore pressure for every cycle, and they observed the characteristic concave downward followed by concave upward shape for the generation of excess pore pressure. However, in this study, an attempt is made to predict the threshold number of cycles by incorporating the stiffness degradation and the mean excess pore pressure.

To estimate the critical number of cycles, the degradation index curves are plotted along with the mean excess pore pressure curves. The specimens which fluidize show a rapid reduction in the stiffness (Fig. 4a) that is accompanied by a sharp rise in the mean excess pore pressures. The point of intersection of the two curves can be defined as the threshold number of cycles, N_{thr}, initiating the onset of fluidization. It is important to note that N_{thr} differs from the critical number of cycles, N_c as defined by Indraratna et al. 2020b, as it considers stiffness degradation and pore pressure response of the fluidized specimens as opposed to mere axial strain response. As shown in Fig. 4, when the specimen compacted at ρ_d = 1790 kg/m^3 is subjected to a CSR of 0.5 and frequency of 1.0 Hz, the degradation index at 5% cyclic axial strain (ε_{ac}) is about 0.46, and the mean excess pore pressure accumulated at the end of the test (i.e. at ε_{ac} = 5%) is 0.63. The threshold number of cycles, N_{thr}, can be estimated as N_{thr} =

50. Similarly, the values of the threshold number of cycles required for the onset of subgrade fluidization at various loading conditions are summarised in Table 2.

4.2. Evaluating threshold residual axial strain, $\varepsilon_{ar,thr}$

The residual axial strain corresponding to the threshold critical number of cycles is denoted as $\varepsilon_{ar,thr}$. Referring to Fig. 4b, it is noted that the present methodology of estimating N_{thr} overestimates the critical number of cycles N_c, as obtained from the inflexion point on the concave axial strains plots (Indraratna et al. 2020b). It could be attributed to the fact that the determination of N_c, did not take into account the stiffness degradation of the specimen and captured only the point of rapid axial strain accumulation. Also, one can observe that there is a quasi-linear relationship between $\varepsilon_{ar,thr}$ and $\log(N_{thr})$ at a given cyclic stress ratio. The threshold residual axial strain corresponding to different CSR, loading frequency and RC is shown in a single plot (Fig. 4c). The specimen compacted at an RC = 93% has a lower value of the threshold axial strain at CSR = 0.5 (i.e., 1.2%) compared to the specimen compacted at RC = 99% (i.e., 1.6%) when subjected to a loading frequency of 1.0 Hz. However, it is interesting to note that the loose specimen (i.e., RC = 93%) fails quicker than the relatively dense specimen (RC = 99%) attributed to the rapid generation of excess pore pressure in the loose specimen. Moreover, as the smaller loading frequency imparts higher residual axial strains for the fluidized specimens (discussed in above section 3.2.), the threshold residual axial strains follow the same trend (Fig. 4c). In order to compare the variation of the threshold axial strains for fluidized specimens, the above procedure was repeated for soil-MP2 which fluidized under undrained cyclic loading (Indraratna et al. 2020a). In particular, $\varepsilon_{ar,thr}$ decreases faster with N given the same frequency f = 5.0 Hz. The difference in the relative compaction of the two soils (both having very different fines content) could be the reason for the relatively flatter behaviour for the current soil (Fig. 5a).

The threshold axial strains were also evaluated for the undrained cyclic triaxial tests on the ultrasoft and medium plastic soil (w_{LL} = 54.9%; PI = 27.5; cohesion, c = 7.58 kPa) reported by Lei et al. (2016). The CSR reported by them was computed using the ratio of the applied dynamic stress to the effective confining pressure. Therefore, the soil that exhibited instability at a CSR of 0.35 by Lei et al., (2016) could be re-evaluated to a CSR of 0.175 based on the definition consistent with Eq. (1) of the current paper. It is noted that Lei et al. (2016) have observed an inflection point in the behaviour of the soft soil with respect to frequency by subjecting the soil specimens to a frequency range of 1.0 to 10.0 Hz. However, no such inflection point can be observed in the present study for the tested loading frequency range of 1.0-5.0 Hz, but the variation in the threshold residual axial strain matches well with the trend reported by Lei et al. (2016) as shown in Fig. 5b.

5. Discussion and practical implications

By carrying out undrained cyclic triaxial testing, the critical cyclic stress ratio (CSR_c) at which the specimen fluidise can be determined. Based on the test results, it is evident that the subgrade soil specimens undergo severe stiffness degradation when the applied CSR exceeds the CSR_c which was also reported by other researchers (Zhou and Gong 2001; Leng et al. 2017). The threshold number of cycles, N_{thr}, corresponds to the point where the increasing mean excess pore pressure ratio and the decreasing stiffness degradation index meet. It provides an estimate to the minimum number of cycles required to initiate rapid axial strain accumulation in the specimen. The threshold residual axial strain corresponding to the N_{thr}, marks the onset of fluidisation for the test specimens. The methodology adopted above is highlighted in Fig. 6.

It is noted that the above method is yet to be applied for a wide range of soils to further strengthen the correlation between the generation of mean excess pore pressure and stiffness degradation. However, the current analysis shows promising results for low to medium plastic clays (Indraratna et al. 2020a and 2020b). Further, the role of principal stress rotation on the stiffness degradation is yet to be investigated. It is believed that the principal stress rotation would aggravate the stiffness degradation and increase the cyclic axial strains (Cai et al. 2018). Moreover, the thresholds would be higher for drained or partially drained than in undrained conditions (Mamou et al. 2019).

6. Conclusions

The present study was focussed on analysing the stiffness degradation of fluidized soil specimens. Based on the present study, the following salient conclusions can be drawn:

- There is a steep decrease in the axial dynamic stiffness of the specimens that are subjected to a higher CSR. For example, when the specimen compacted at an initial density of ρ_d = 1790 kg/m^3 was subjected to a CSR = 0.5 at f = 1.0 Hz, the stiffness reduced to 30% of the initial value in about 100 cycles.
- There exists a near linear relationship between $\varepsilon_{ar,thr}$ and log(N_{thr}) for the tested frequency range (1.0 to 5.0 Hz) and CSR (0.4 to 1.0). However, further experimental data for different soil types is required to establish a more reliable governing relationship that can encompass a wider range of soils that are vulnerable for mud pumping.
- The threshold number of cycles required to initiate fluidization could be evaluated by knowing the stiffness degradation index (δ) and the evolution of the mean excess pore pressure in the specimen. This value of N_{thr} depends on the soil type, gradation, CSR, loading frequency and relative compaction. N_{thr} predicted from the above methodology seems to overestimate the critical number of cycles N_c, obtained from the inflexion point of the concave axial strain plots.

Acknowledgements

This research was supported by the Australian Government through the Australian Research Council's Linkage Projects funding scheme (project **LP160101254**) and the Industrial Transformation Training Centre for Advanced Technologies in Rail Track Infrastructure (ITTC), University of Wollongong. The authors also acknowledge the support from Transport Research Centre, University of Technology Sydney, Australia.

List of Notations:

CSR	Cyclic stress ratio
CSR_c	Critical cyclic stress ratio
$E_{d,N}$	Axial dynamic modulus
f	Loading frequency
G_s	Specific gravity
k_0	Ratio of effective horizontal stress to the vertical stress
N_c	Critical number of cycles
N_{thr}	Threshold number of cycles
PI	Plasticity index
q_0	Initial deviatoric stress
RC	Relative compaction
u_m/σ'_{3c}	Mean excess pore pressure ratio
w_{LL}	Liquid limit
δ	Stiffness degradation index
ε_{ac}	Cyclic axial strain
$\varepsilon_{ar,thr}$	Threshold residual axial strain
ρ_d	Initial dry density
σ'_{3c}	Effective confining pressure after consolidation
σ_d	Applied cyclic stress

Tables

Table 1 Basic geotechnical properties of the soils analysed in this study

Characteristics of sub-soil	**Soil – MP1** (present study)	**Soil – MP2** (Indraratna et al., 2020a)
Liquid limit, w_{LL}	26%	25%
Plasticity index, PI	11%	10%
Initial moisture content	15%	20%
Specific Gravity, G_s	2.63	2.65
USCS Classification	CL	CL
Maximum dry density, $\rho_{d,max}$ (kg/m^3)	1814	1820
Finer fraction (< 75 μm)	30%	54%

Table 2 Summary of the threshold number of cycles N_{thr} and threshold residual axial strains $\varepsilon_{ar,thr}$ for different loading conditions

Soil	**Initial Density**	**Relative Compaction**	**CSR**	***f* (Hz)**	N_{thr}	$\varepsilon_{ar,thr}$ (%)
Soil - MP1 (Present study)	1790	99%	0.5	1.0	50	1.6
				2.0	240	1.4
				5.0	3300	0.95
			1.0	1.0	10	1.75
				2.0	22	1.5
				5.0	40	1.3
	1680	93%	0.4	1.0	310	1.05
			0.5	1.0	11	1.2
				2.0	100	0.7
Soil - MP2 (Indraratna et al., 2020a)	1710	94%	0.3	5.0	58	0.52
			0.4		33	0.9
			0.5		12	1.3

Figures

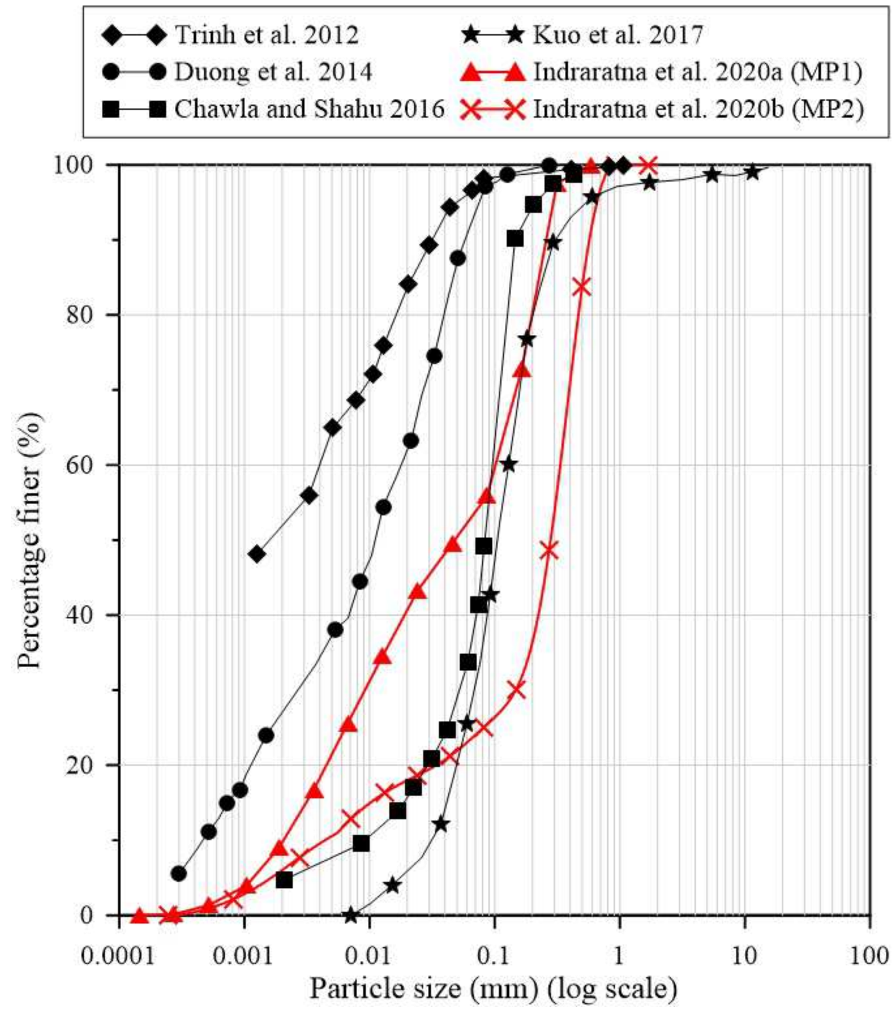

Fig. 1 Particle size distribution of subgrade soils reported to have mud pumped in the field

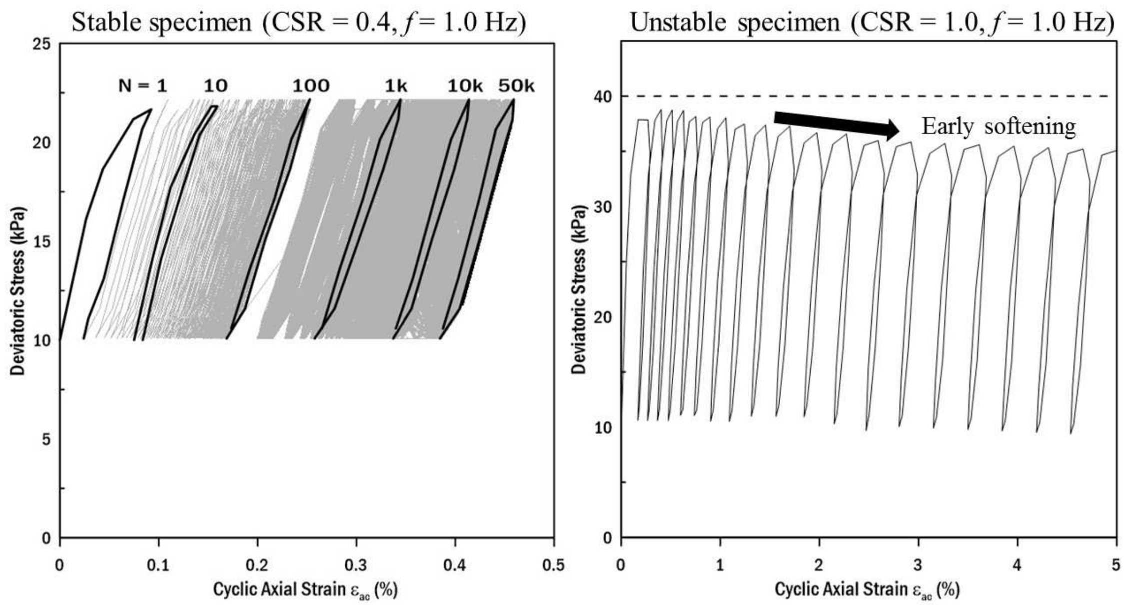

Fig. 2 Stress-strain loops for the stable (low CSR) and unstable specimen (high CSR)

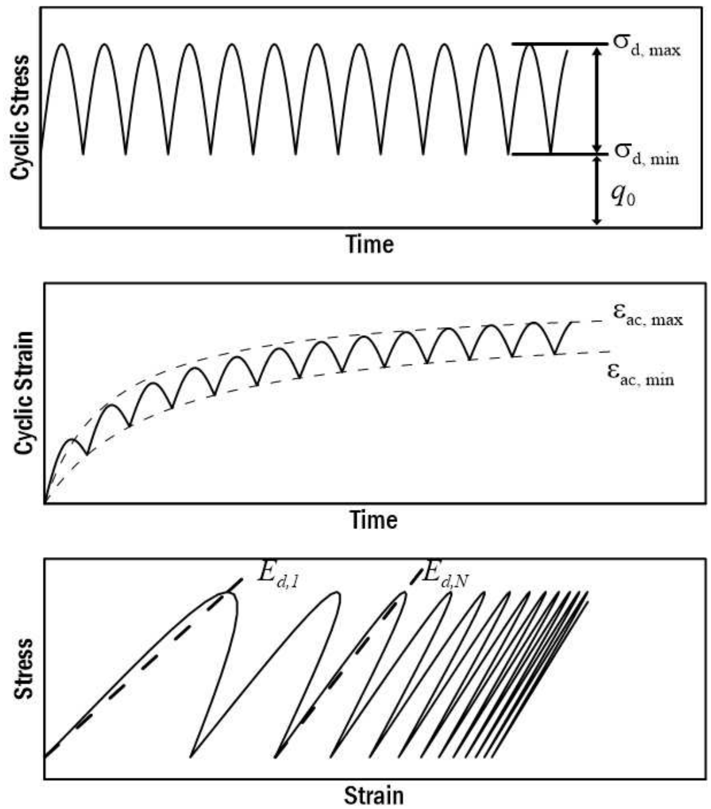

Fig. 3 Generalized stress-strain behaviour for a specimen subjected to one-way stress-controlled cyclic loading under undrained condition

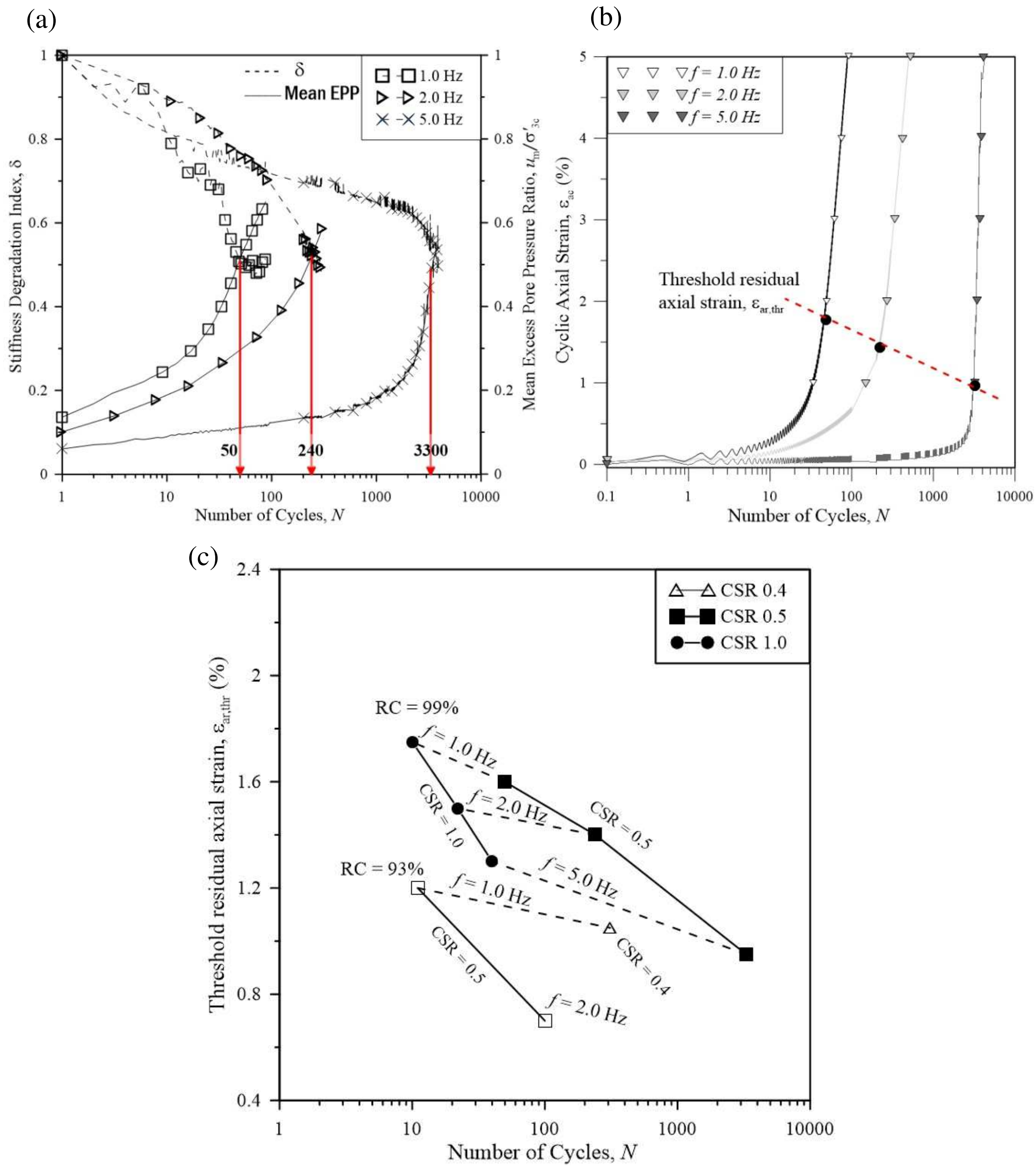

Fig. 4 (a) Predicting the threshold number of cycles N_{thr}, from the degradation index and mean EPP plots (b) Evaluating threshold residual axial strains (ρ_d = 1790 kg/m^3, CSR = 0.5) (c) Threshold residual axial strain for various loading conditions for Soil – MP1

(a)

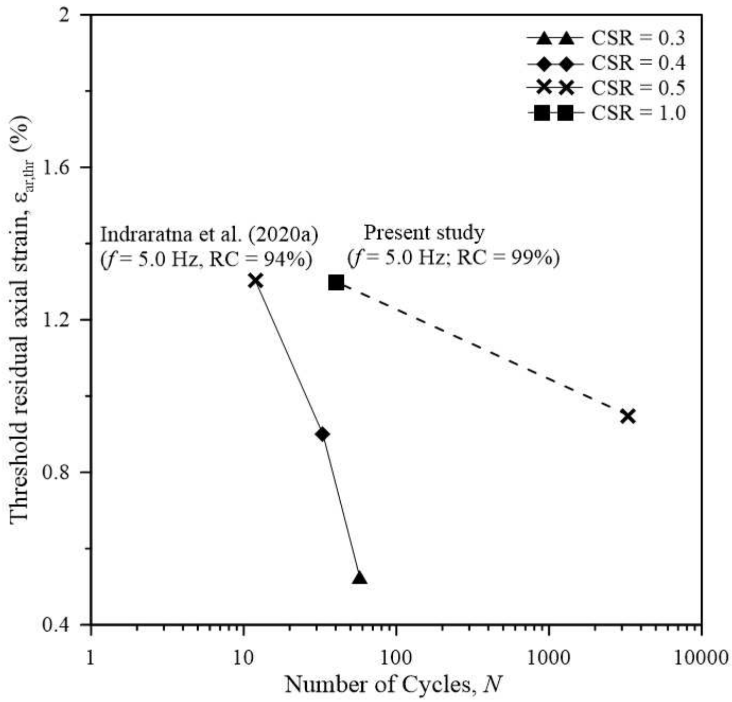

(b)

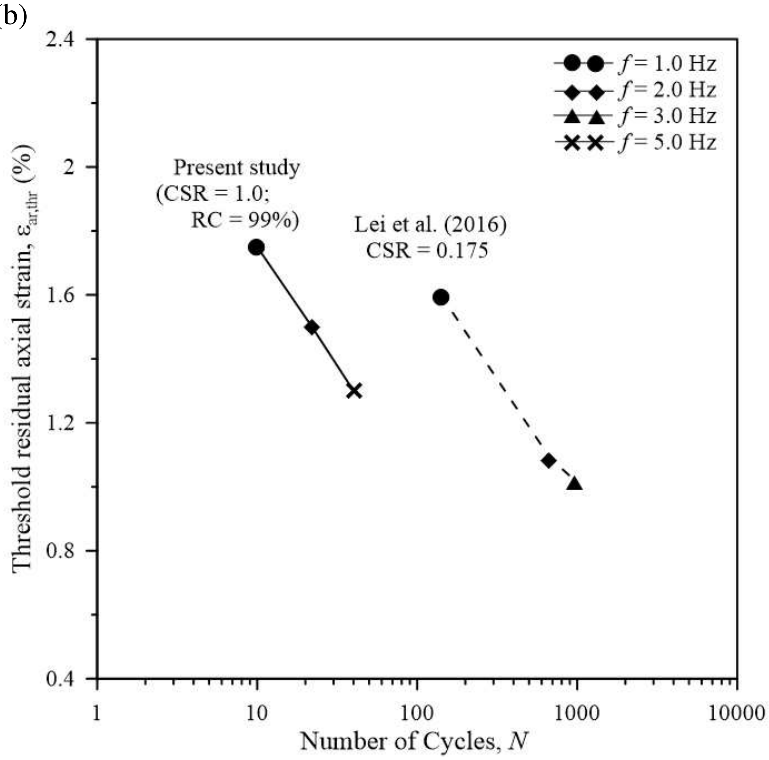

Fig. 5 Comparison of the threshold axial strains (a) for the two soils (Soil-MP1 and Soil-MP2) at f = 5.0 Hz (b) with respect to different loading frequency

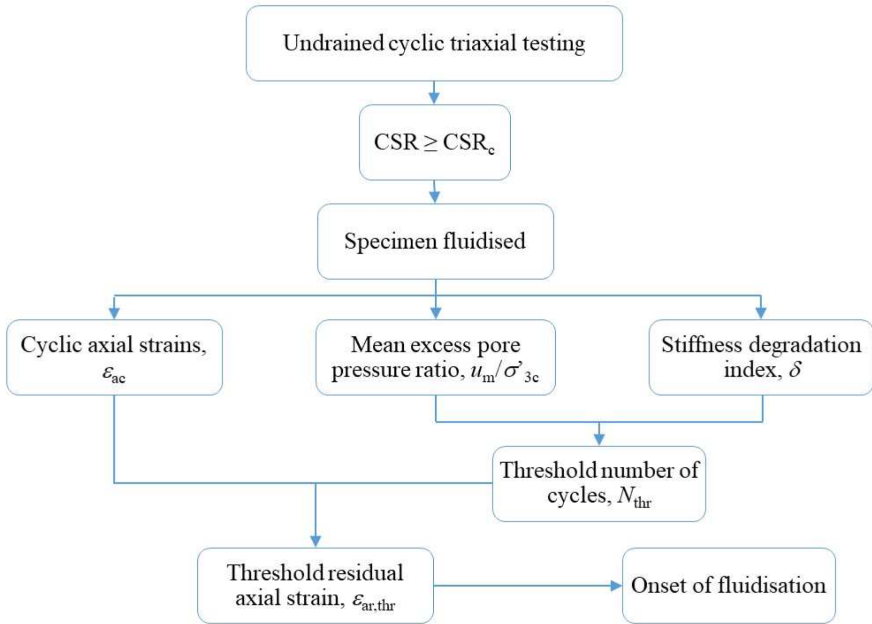

Fig. 6 Flowchart for predicting the onset of fluidisation for mud pumping prone soils using stiffness degradation index

References:

ASTM D698-07 Standard. 2012. Standard Test Methods for Laboratory Compaction Characteristics of Soil Using Standard Effort.

Cai, Y., Wu, T., Guo, L. and Wang, J. 2018. Stiffness degradation and plastic strain accumulation of clay under cyclic load with principal stress rotation and deviatoric stress variation. Journal of Geotechnical and Geoenvironmental Engineering, **144**(5): 04018021.

Chawla, S. and Shahu, J.T. 2016. Reinforcement and mud-pumping benefits of geosynthetics in railway tracks: Model tests. Geotextiles and Geomembranes, 44: pp. 366-380.

Duong, T.V., Cui, Y.-J., Tang, A.M., Dupla, J.-C., Canou, J., Calon, N., Robinet, A., Chabot, B. and De Laure, E. 2014. Physical Model for Studying the Migration of Fine Particles in the Railway Substructure. Geotechnical Testing Journal, 37(5): pp. 1-12.

Hasnayn, M.M., McCarter, W.J., Woodward, P.K. and Connolly, D.P. 2020. Railway Subgrade Performance after Repeated Flooding Large-scale Laboratory Testing. Transportation Geotechnics. doi: 10.1016/j.trgeo.2020.100329

Hasnayn, M.M., McCarter, W.J., Woodward, P.K., Connolly, D.P. and Starrs, G. 2017. Railway subgrade performance during flooding and the post-flooding (recovery) period. Transportation Geotechnics, **11**: 57-68. doi: 10.1016/j.trgeo.2017.02.002

Hsu, C.-C. and Vucetic, M. 2006. Threshold shear strain for cyclic pore-water pressure in cohesive soils. Journal of Geotechnical and Geoenvironmental Engineering, **132**(10): 1325-1335.

Indraratna, B., Korkitsuntornsan, W. and Nguyen, T.T. 2020a. Influence of kaolin content on the cyclic loading response of railway subgrade. Transportation Geotechnics, **22**: 100319. doi: https://doi.org/10.1016/j.trgeo.2020.100319.

Indraratna, B., Singh, M., Nguyen, T.T., Leroueil, S., Abeywickrama, A., Kelly, R. and Neville, T. 2020b. Laboratory study on subgrade fluidization under undrained cyclic triaxial loading. Canadian Geotechnical Journal. doi: https://doi.org/10.1139/cgj-2019-0350.

Kallioglou, P., Tika, T. and Pitilakis, K. 2008. Shear modulus and damping ratio of cohesive soils. Journal of Earthquake Engineering, **12**(6): 879-913.

Konstadinou, M. and Georgiannou, V.N. 2014. Prediction of pore water pressure generation leading to liquefaction under torsional cyclic loading. Soils and Foundations, **54**(5): 993-1005. doi: https://doi.org/10.1016/j.sandf.2014.09.010.

Kuo, C., Hsu, C., Wu, C., Liu, P. and Chen, D. 2017. Study on the Piping Path and Mechanism of Mud-pumping in Railway Subgrade. 19th International Conference on Soil Mechanics and Geotechnical Engineering. Seoul, South Korea.

Lei, H., Li, B., Lu, H. and Ren, Q. 2016. Dynamic Deformation Behavior and Cyclic Degradation of Ultrasoft Soil under Cyclic Loading. Journal of Materials in Civil Engineering, ASCE, **28**(11): 04016135. doi: doi:10.1061/(ASCE)MT.1943-5533.0001641.

Leng, W., Xiao, Y., Nie, R., Zhou, W. and Liu, W. 2017. Investigating strength and deformation characteristics of heavy-haul railway embankment materials using large-scale undrained cyclic triaxial tests. International Journal of Geomechanics, **17**(9): 04017074.

Liu, J. and Xiao, J. 2010. Experimental study on the stability of railroad silt subgrade with increasing train speed. Journal of Geotechnical and Geoenvironmental Engineering, 136(6): 833-841.

Mamou, A., Clayton, C., Powrie, W. and Priest, J. 2019. The role of clay content on the response of railway track foundations during free-to-drain cyclic changes in principal stress rotation. Transportation Geotechnics. **20**: (100246). doi.org/10.1016/j.trgeo.2019.100246

Mortezaie, A.R. and Vucetic, M. 2013. Effect of Frequency and Vertical Stress on Cyclic Degradation and Pore Water Pressure in Clay in the NGI Simple Shear Device. **139**(10): 1727-1737. doi:10.1061/(ASCE)GT.1943-5606.0000922.

Nguyen, T.T. and Indraratna, B. 2020. A coupled CFD-DEM approach to examine the hydraulic critical state of soil under increasing hydraulic gradient. ASCE International Journal of Geomechanics, 20(9): 04020138-1:15. doi: https://doi.org/10.1061/(ASCE)GM.1943-5622.0001782.

Nguyen, T.T., Indraratna, B., Kelly, R., Phan, N.M. and Haryono, F. 2019. Mud pumping under railtracks: mechanisms, assessments and solutions. Australian Geomechanics Journal, **54**(4): 59-80.

Powrie, W., Yang, L. and Clayton, C.R. 2007. Stress changes in the ground below ballasted railway track during train passage. Proceedings of the Institution of Mechanical Engineers, Part F: Journal of Rail Rapid Transit, **221**(2): 247-262.

Singh, M., Indraratna, B. and Rujikiatkamjorn, C. 2019. Use of geosynthetics in mitigating the effects of mud pumping: a railway perspective. *In* Geotechnics for transportation infrastructure. *Edited by* R. Sundaram, Shahu, J. & Havangi, V. Springer, Singapore.

Soralump, S. and Prasomsri, J. 2016. Cyclic pore water pressure generation and stiffness degradation in compacted clays. Journal of Geotechnical and Geoenvironmental Engineering, **142**(1): 04015060.

Trinh, V.N., Tang, A.M., Cui, Y.-J., Dupla, J.-C., Canou, J., Calon, N., Lambert, L., Robinet, A. and Schoen, O. 2012. Mechanical characterisation of the fouled ballast in ancient railway track substructure by large-scale triaxial tests. Soil and Foundations, The Japanese Geotechnical Society, 52(3): pp. 511-523.

Zhou, J. and Gong, X. 2001. Strain degradation of saturated clay under cyclic loading. Canadian Geotechnical Journal, **38**: 208-212.